Nucl Med Mol Imaging (2011) 45:103–110
DOI 10.1007/s13139-011-0076-x

ORIGINAL ARTICLE

Total Thyroidectomy in the Mouse: the Feasibility Study in the Non-thyroidal Tumor Model Expressing Human Sodium/Iodide Symporter Gene

Hye-kyung Shim · Seog Gyun Kim · Tae-Sung Kim · Seok-ki Kim · Sang Jin Lee

Received: 30 June 2010 / Accepted: 24 January 2011 / Published online: 15 February 2011
© Korean Society of Nuclear Medicine 2011

Abstract
Purpose This study sought to probe the feasibility of performing total thyroidectomy in the mouse using a non-thyroidal hNIS expressing tumor model.
Materials and Methods Our thyroidectomy protocol included thorough excision of both lobes and the isthmus. For evaluating the completeness of thyroidectomy, we compared the ^{99m}Tc-pertechnetate scans taken before and after thyroidectomy. The prostate cancer cell line was subcutaneously inoculated 2 weeks after the thyroidectomy. When the tumor reached 5-10 mm in diameter, Ad5/35-E4PSESE1a-hNIS was injected intratumorally, and ^{131}I scans were performed. The radioiodine uptakes of the neck and the tumor were compared with those of the other regions.
Results Total thyroidectomy was performed in 13 mice. Although 38.5% died during or just after thyroidectomy, the others survived in good health for 2 months. Thyroid tissue was completely eliminated using our protocol; the residual uptake of ^{99m}Tc-pertechnetate was minimal in the neck area. The neck/background uptake ratio after thyroidectomy was significantly lower than that before thyroidectomy ($p<0.05$). Non-thyroidal tumor models were successfully established in all the surviving mice. Radioiodine accumulation in the tumors was visualized on ^{131}I scans, and the neck uptakes were minimal.
Conclusion Using our total thyroidectomy protocol, we successfully established a hNIS-transfected prostate cancer model with a minimal accumulation of radioiodine in the neck. The relatively high mortality after surgery can be a problem, and this might be reduced by minimizing the surgical stress.

Keywords Mouse · Total thyroidectomy · Surgical technique · Human sodium/iodide symporter

H.-k. Shim · S. G. Kim · T.-S. Kim · S.-k. Kim (✉) · S. J. Lee
Hospital and Research Institute, National Cancer Center,
323 Ilsan-ro, Ilsandong-gu, Goyang-si,
Gyeanggi-do 410-769, Republic of Korea
e-mail: skkim@ncc.re.kr

Introduction

The human sodium/iodide symporter (*hNIS*) plays an important role in the biosynthesis of thyroid hormones as it mediates the active transport of iodide into thyrocytes [1–3]. By targeted transfer and expression of the *hNIS* gene, radioiodine treatment could be used to treat non-thyroid malignant disease as well as thyroid carcinoma [4–6]. In case of assessing the *hNIS* gene expression in a xenograft mouse model, intense radioiodine accumulation in *hNIS*-expressing organs such as the thyroid is deterrent to scintigraphic assessment.

In vivo experiments are mandatory in basic research and must be performed prior to considering human clinical trials. Mouse models have gained popularity for a number of reasons, such as small body size, rapid gestation period, relatively low maintenance costs, and an extensively characterized genome [7]. However, reports of mouse thyroidectomy are not as common as those of thyroidectomy in the rat, conceivably because of the difficulty of the microsurgical technique.

In this study, we tried to refine the total thyroidectomy technique; the surgical accomplishment was confirmed by a scintigraphic scan. We then utilized totally thyroidectomized mice to image *hNIS*-transfected prostate cancer cells and identified the feasibility of our thyroidectomy protocol.

Materials and Methods

Animals

A total of 13 mice (BALB/c-*nu*), ages 7 to 9 weeks and weighing approximately 16–21 g, were purchased from Japan SLC, Inc. The mice were housed and maintained in individually ventilated cage under specific pathogen-free conditions in facilities. The mice were used in accordance with the Animal Care and Use Guidelines of the National Cancer Center, Institute, and Hospital under the protocol approved by the Institutional Animal Care and Use Committee.

Operation

Animals were anesthetized by using 2% isoflurane in 100% oxygen through nose-cone masks. All animals were placed in the supine position with the neck elevated by rolled-up sterilized gauze. Operations were carried out under aseptic conditions. Surgical tools and draping linens were autoclaved prior to the surgery. The operating field was disinfected with betadine solution and 70% alcohol. The betadine was applied to neck of the mouse, and animals were draped under the microscope (Leika, EZ4, German), leaving only the operating field exposed to prevent contamination of the surgical site during the operation. A set of sterile gloves was used for each mouse.

To test the anesthesia's depth before operation, a paw of the mouse was squeezed firmly without injuring it. If the mouse did not withdraw its leg, the surgery was started. An anterior neck incision was made vertically. The parotid glands beneath the skin occupied almost all the anterior neck space. Each of the parotid glands was separated laterally while gently grasping with non-traumatic forceps (Fig. 1a). After transparent investing fascia upon the strap muscle was removed, bilateral strap muscles were retracted laterally and held by retractors. Through the transparent pretracheal fascia, bilateral thyroid lobes were visualized along with the transparent isthmus in front of the trachea (Fig. 1b). Thyroid glands are usually located between the cricoid cartilage and first four tracheal rings.

The isthmus was transected by microdissecting forceps, and each side of the lobes was then gently teased away from the trachea. (Fig. 1c, d, and Fig. 2 a, b). As the bilateral thyroid upper poles are located near the insertion of the sternothyroid muscle, thyroids are easily torn in this area when dissected. Therefore, sternothyroid muscles before removing thyroid lobes (Fig. 2c) should be retracted upward laterally along with strap muscles before thyroidectomy or gently picked up with forceps when the bilateral thyroid upper poles are removed. Care was taken

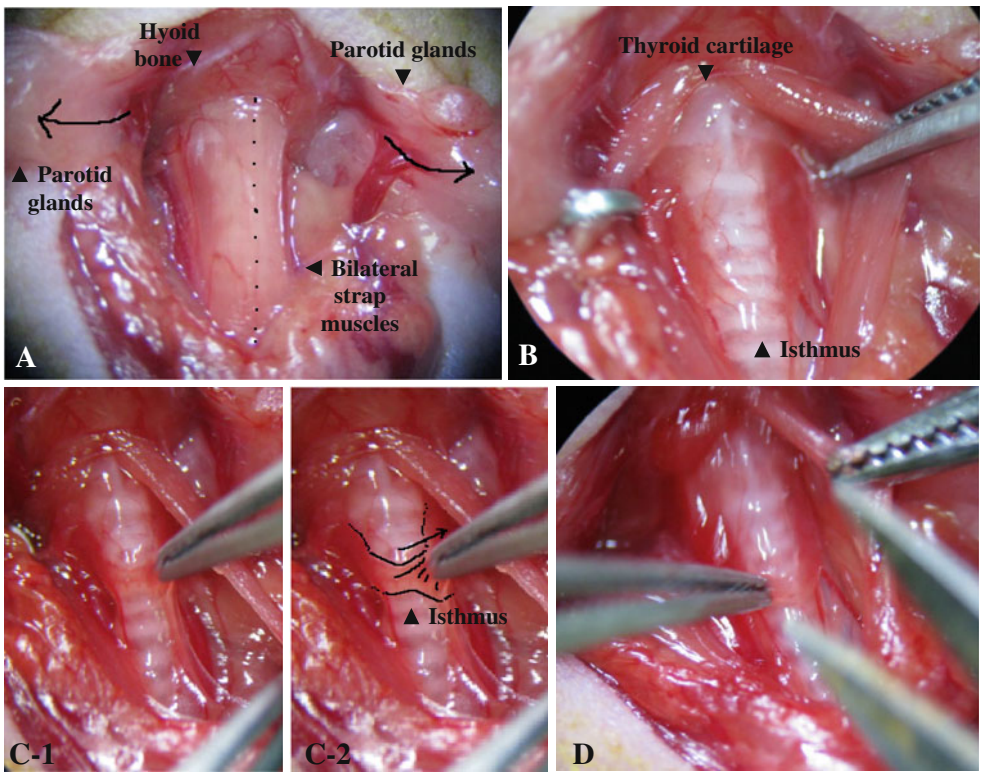

Fig. 1 Bilateral parotid glands were gently divided along the midline and placed laterally upon the skin, and bilateral strap muscles were then exposed under the investing fascia (**a**). Bilateral sternocleidomastoid muscles were also exposed in this image. Thyroid cartilage and the hyoid bone were visualized along with multiple tracheal rings in this figure (**b**). The figure shows bilateral thyroid glands with a flat and transparent isthmus. The isthmus was pulled up with forceps (**c**-1, **c**-2) and cut vertically (**d**)

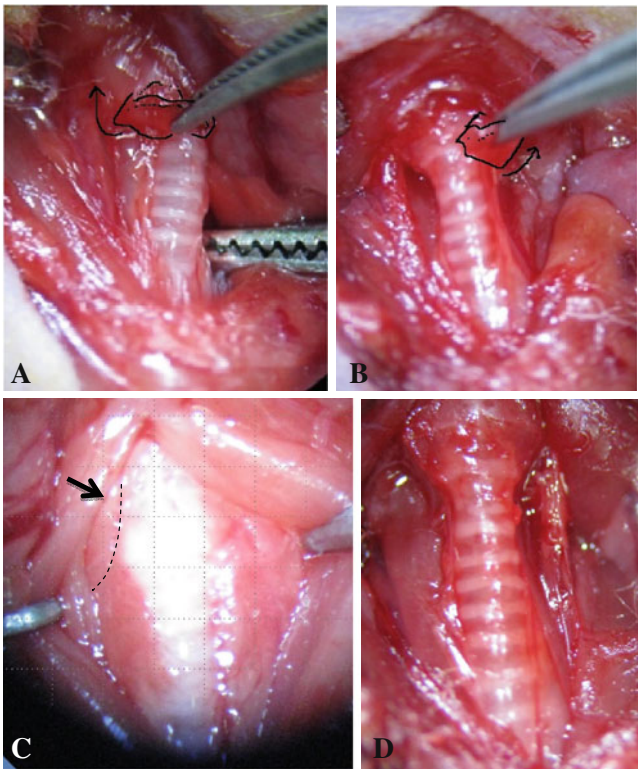

Fig. 2 Upon cutting in half with scissors in the isthmus, the bilateral lobes of the thyroid were grasped on the medial side and dissected upward and laterally (**a**, **b**). The sternothyroid muscles were located in the upper pole of bilateral lobes (**c**), which were retracted along with the strap muscles before dissecting. Minor bleeding was easily controlled by gentle pressure with a piece of cotton. After total thyroidectomy, the trachea was visualized without the thyroids (**d**). After saline irrigation, musculature, lymphatic tissues and parotid glands were repositioned, and skin was sutured

not to injure the recurrent laryngeal nerve, which runs below the dorsal edge of the thyroid lobes (Fig. 3a, b). The risk of major bleeding was not high because all major vessels are located inside a carotid sheath (Fig. 3c). After irrigation of the surgical field with normal saline, musculature, lymphatic tissue, and salivary glands were repositioned, and the skin was closed with 4-0 silk suture. The surviving mice were observed until 1 month after surgery for examining survival and performance status.

After applying betadine to the anterior neck, oxygen supplementation by a mask was administered under a warming lamp until the mice were able to move actively. Once fully awake, the animals were given access to 1% calcium gluconate (Choong Wae Pharmaceutical, Ltd., South Korea) to prevent hypothyroidism and normal mouse chow [5]. Excised thyroid lobes were fixed with 10% formalin, washed with distilled water, and dehydrated in 70% ethanol. The specimen was sliced into 4-μm-thick sections and embedded in paraffin. Hematoxylin and eosin (H&E) staining was performed, and the examination was done under a light microscope (×40, ×100, and ×400 magnification).

The Preoperative and Postoperative ^{99m}tc-Pertechnetate Whole Body Scan and Region of Interest Drawing

All animals were injected with 500 Ci ^{99m}Tc-pertechnetate intraperitoneally. After 30 min, basal whole body ^{99m}Tc-pertechnetate static imaging was done by using a small animal SPECT system (nanoSPECT/CT, Bioscan Inc., Washington, DC). In 30–60 min, the total thyroidectomy was done and 1 h after intraperitoneal injection, a second scintigraphic image was taken to evaluate remnant tissue. The scintigraphic acquisition and processing were performed using a parallel-hole collimator, with a zoom factor of 1.14 and a 512 × 512 matrix size until reaching 80,000 counts. Circular or elliptical regions of interest (ROI) were drawn on the neck, stomach, and bladder, and an ROI drawing along the whole body was also done for quantifying background activity (Fig. 4a). The thyroid/corrected background count (CBC) ratio was calculated to account for variable, and sometimes very intense, physiologic radiolabel uptake in the stomach and bladder (CBC= whole body count-neck count-bladder count-stomach count) (Fig. 4b, c).

Cwr22rv Cell Injection and Viral Treatment, Radioiodine In Vivo Imaging

A prostate-restricted replication-competent recombinant adenovirus serotype 5/35 construct (Ad5/35E4PSESE1a-hNIS) carrying human NIS under the control of the PSES promoter was constructed. Ad5/35E4PSESE1a-hNIS was constructed by using Ad-E4PSESE1a as a backbone, which was previously described in detail [8].

Androgen-independent human prostate cancer cell line CWR22rv was derived from an androgen-dependent human xenograft tumor, CWR22. Adherent monolayer cultures were maintained in culture flasks (BD Bioscience) and incubated at 37°C in 5% carbon dioxide and 95% air. As recommended, the cells were cultured in RPMI1640 supplemented with 10% FBS and 100 U antibiotic-antimycotic solutions (Invitrogen). The cells suspended with PBS were injected subcutaneously into the right shoulder (1×10^6 cells) of all surviving mice (8 thyroidectomy mice).

When the tumor reached to 5–10 mm, it was treated with the Ad5/35-E4PSESE1a-hNIS (5×10^8 PFU) through intratumoral injections on 2 consecutive days. Intratumoral injections were done slowly for 10 s at multiple sites in order to facilitate viral dispersal, using a 30-gauge needle in a total volume of 50 μl of PBS. All injections were done under anesthesia with inhalation of 2% isoflurane. Twenty-

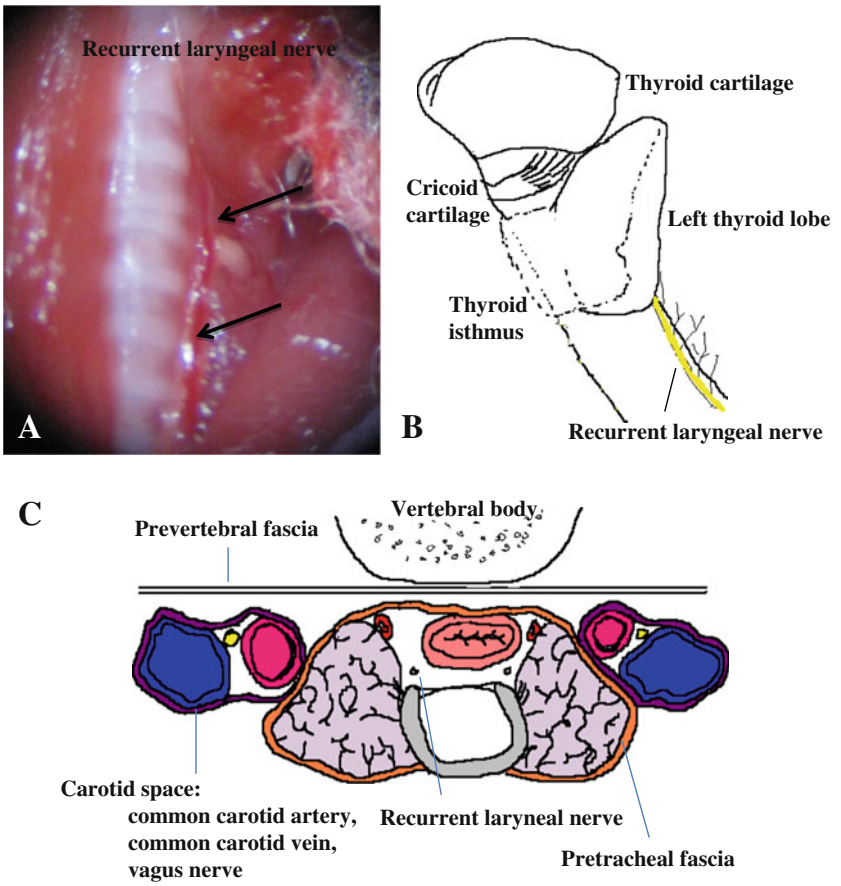

Fig. 3 Under the medial side of the bilateral thyroids at the tracheoesophageal groove, the recurrent laryngeal nerve was visible along with a draining vein (**a** arrow, **b** yellow line). (**c**) shows the compartments of the neck. The thyroids were anatomically grouped with the trachea, esophagus, feeding artery, and bilateral recurrent laryngeal nerves inside the pretracheal fascia. The common carotid artery, vein, and vagus nerves were in the carotid space. The vertebral body was divided by prevertebral fascia with the anterior structure. By identifying these anatomies, massive bleeding can be prevented

four hours after the last viral injection, mice received 0.5 mCi (18.5 MBq) of ^{131}I-NaI intravenously, followed by imaging using a γ-camera with a pin-hole collimator (DSX, Argus) 12 h after radioiodine injection. The scan parameters were as follows: pin-hole diameter, 5 mm; distance, 2 cm apart from mouse; scanning time, 5 min/scan; γ-energy window, 364 keV±20 %; matrix size, 256×256×16.

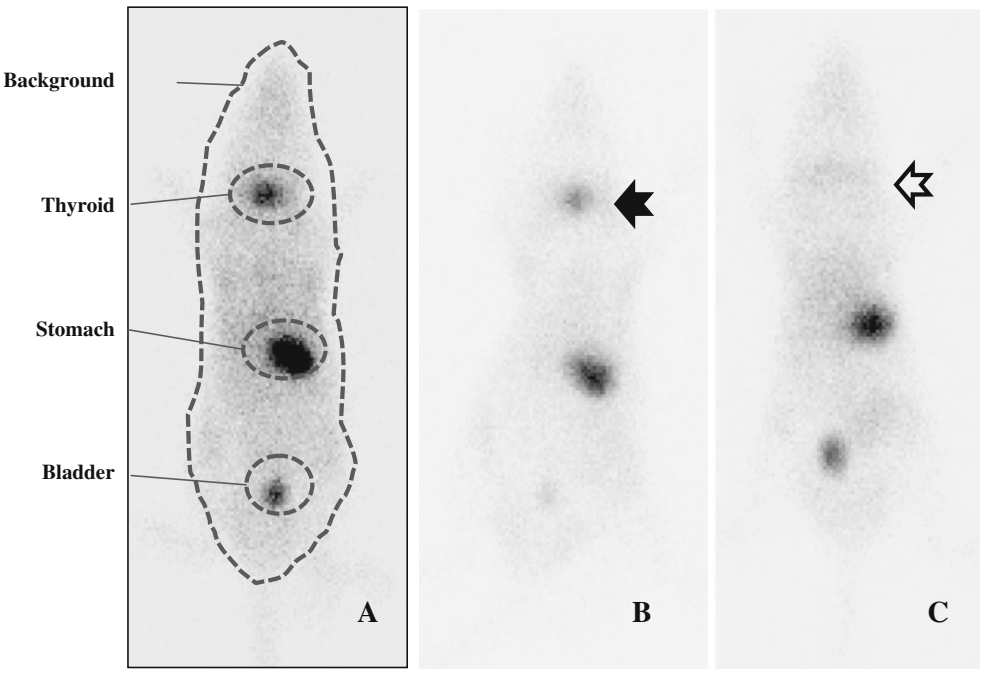

Fig. 4 The ^{99m}Tc-pertechnetate whole-body scans were done for each mouse in the small animal SPECT system. (**a**) represents the regions of interest in the neck, stomach, bladder, and total body. For background correction, remnant thyroid/corrected background (whole body-remnant thyroid-stomach-bladder, if visible) was calculated. (**b**) shows intense radiolabel uptake in the neck area before surgery (black arrow). (**c**) shows the image taken after total thyroidectomy. Compared with the preoperative scan, the postoperative scan shows faint remnant radiolabel uptake

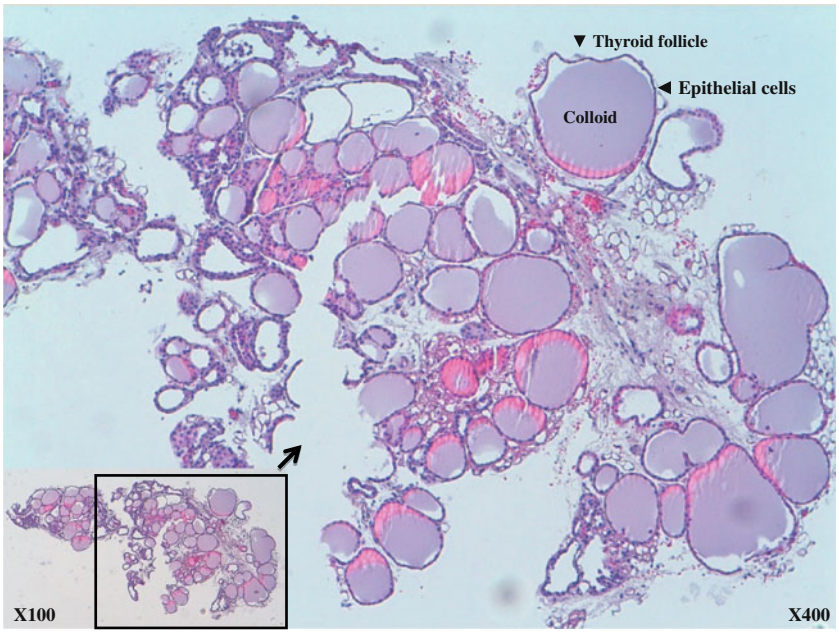

Fig. 5 The removed thyroid glands were stained with hematoxylin and eosin (H&E), and examined under the microscope. The ×100 image in the lower right square box is included, and part of the image is enlarged to ×400 magnification. The glands were composed of many spherical hollow sacs called thyroid follicles. In this tissue section, each follicle appeared as an irregular circle of cells. These follicles were filled with colloids. The stromal structures were visible between the colloids

Statistical Analysis

Indices associated with thyroids, remnant thyroid activity, stomach, bladder, and thyroids or remnant thyroid activity/CBC ratios between the two groups (pre-surgical scan versus post-surgical scan) were compared using Student's *t*-test. *P* value less than 0.05 was assumed to be significant.

Results

Feasibility and Surgical Success Rate

The operation time ranged from 13–23 (17±3.5) min. Total mortality was 38.5% (5/13). Once a mouse was awakened quickly after cessation of anesthesia and moved around actively, the animals did not die until 2 months after the operation. Some mice died immediately after surgery (n=2) or were not active after surgery (n=3), conceivably because of surgical stress. The awakened mice with poor performance status eventually died by 2 days after surgery. There was no evidence of hemorrhage or sign of inflammation in the thyroid bed of the dead animals, and the bilateral recurrent nerves were all intact.

Excised tissue was identified as a thyroid specimen under a light microscope (×100 and ×400 magnification); there were numerous colloid-containing follicles of varying sizes lined by epithelial cells (Fig. 5). The stromal structures were visible between the colloids.

^{99m}Tc Whole-Body Scan and ROI Analysis

Total thyroidectomy mice showed minimal residual radioiodine uptake in the neck compared with that observed in the pre-surgical scan (Fig. 4b, c, Table 1). For background correction, whole-body radioactivity was measured, and the neck uptake was then divided by corrected background activity. The neck radioactivity was significantly lower in

Table 1 The ROI analysis between pre-surgical and post-surgical ^{99m}Tc-pertechnetate scan

Regions of interest (ROI)		Average counts	Standard deviation	Statistical significance
Neck	TT[a]	5,116.8	1,260.7	0.013*
	WT	6,527.7	931.7	
Stomach	TT	16,839.6	3,396.2	0.381
	WT	15,705.1	1,953.6	
Bladder	TT	3,788.9	1,365.2	0.965
	WT	3,826.1	2,107.7	
Whole body	TT	73,928.8	864.5	0.818
	WT	73,833.4	907.2	
Neck/CBC	TT	0.11	0.03	0.023*
	WT	0.14	0.02	

* Regarded as statistically significant (if p<0.05)

[a] Mice with total thyroidectomy

[b] Mice without thyroidectomy

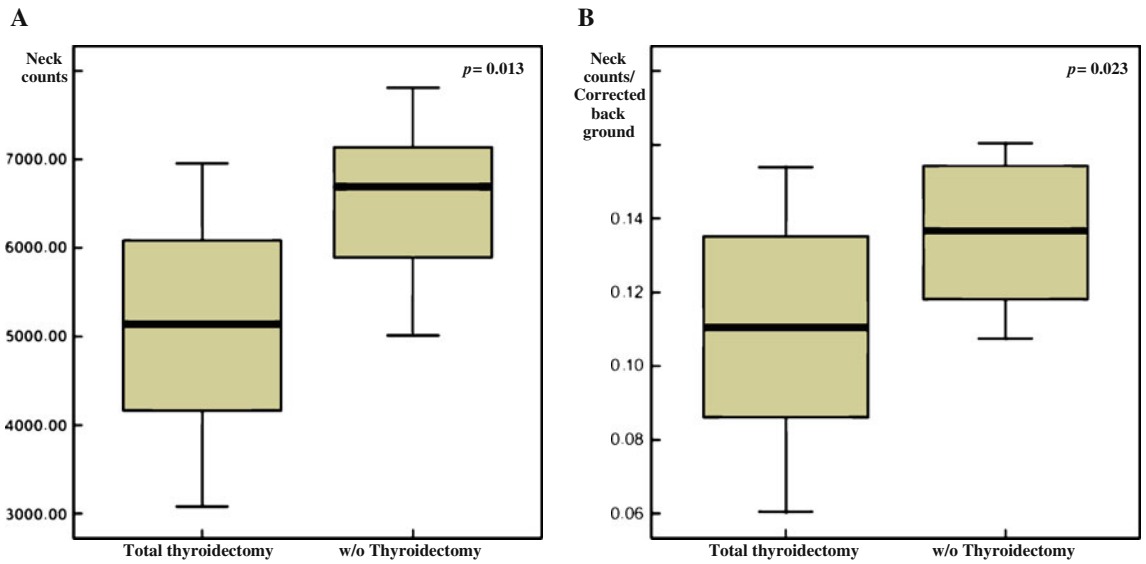

Fig. 6 The neck radioactivity on the postoperative scan was significantly lower compared with that of preoperative scans (5,116.8 ± 1,260.7 versus 6,527.7±931.7, respectively; p=0.013; **a**). The neck/corrected background ratio on the preoperative scan was also significantly lower than that of the postoperative scan (0.11±0.03 versus 0.14±0.12, respectively; p=0.023; **b**)

postoperative images than in preoperative images (5,116.8 ± 1,260.7 and 6,527.7±931.7, respectively; p=0.013). The neck/CBC ratio of the postoperative image was significantly lower than that of the preoperative image (0.11±0.03 and 0.14±0.12, respectively; p=0.023; Fig. 6). However, between the pre- and post-scintigraphic scans, there were no significant differences found in the stomach (16,839.6± 3,396.2 versus 15,705.1±1,953.6; p=0.381), the bladder (3,788.9±1,365.2 versus 3,826.1±2,107.7; p=0.965), and corrected whole body activities (48,183.5±4,194.0 versus 47,774.6±3,100.4; p=0.811) (Table 1).

Radioiodine Imaging of Thyroidectomized Mice with Ad5/35-E4psese1a-Hnis Trasfected Prostate Cancer Tumors

Subcutaneous CWR22rv tumors were established in all mice. In vivo gamma imaging in the early period of radioiodine injection showed that iodine accumulates successfully in the tumor. Radioiodine accumulation into Ad5/35-E4PSESE1a-hNIS-treated tumors was definitely seen 12 h after radioiodine injection. (Fig. 7). Likewise in the immediate postoperative ^{99m}Tc-pertechnetate whole body scan, there was minimal uptake in the neck. Iodine had accumulated in the stomach because of endogenous NIS expression and excreted into the genitourinary system. ^{131}I-NaI in the xenograft accumulated for 24 h and dropped abruptly after 24 h (data not shown).

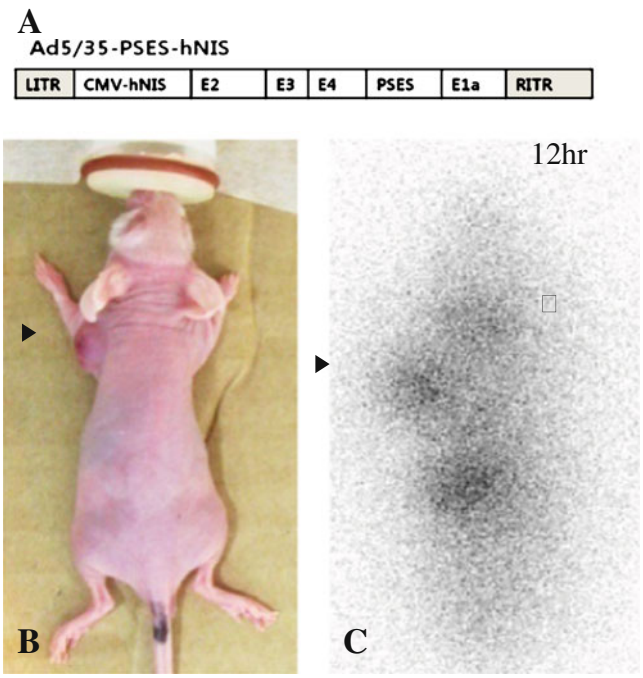

Fig. 7 (**a**) shows a schematic presentation of the virus used in this study. A conditionally replicative virus Ad5/35-PSES-hNIS has CMV-hNIS and PSES-E1a. PSES (prostate-specific enhancer sequence) was inserted in order to control the expression of E1A, which is vital for efficient multiplication. The virus contains chimeric 5/35 fiber, which targets the Ad3 receptor, highly expressed in prostate cancer. (**b** and **c**) represent whole-body ^{131}I-NaI scintigraphy image 12 h after ^{131}I-NaI radionuclide therapy with a compatible image of this mouse. The white arrow represents minimal remnant uptake in the neck, and black arrows show grafted prostate tumor subcutaneously

Discussion

Murine thyroidectomy can be accomplished through surgical excision or radioactive iodine administration. Radioactive

iodine ablation is beneficial in terms of its non-invasiveness; however, complete thyroidectomy is difficult to accomplish and time-consuming. Even though complete thyroidectomy can be fatal because of surgical complications, and the completeness of surgery and surgical complications are operator-dependent, surgical thyroidectomy is the most secure and fastest method to obtain a thyroidectomized mouse model. According to the immediate scintigraphic findings of our thyroidectomized model and successful radioiodine imaging of the grafted *hNIS*-transfected prostate tumor with minimal remnant thyroid uptake, complete thyroidectomy using our protocol is feasible and could be successfully applied to various situations in oncology and endocrinology. The androgen-insensitive prostate cancer that was used in our study is clinically problematic and requires a new treatment modality. Newly developed target chemotherapeutic agents also have limited efficacy, so *hNIS*-gene transfer with radioiodine therapy could be a promising therapeutic tool.

Despite the various surgical instruments and techniques that have been developed, the surgery in mice is still not easy to perform because of the animal's small structure. The difference in anatomy between the mouse and the rat is as follows: The isthmus of mice is small in volume and is rather flat, so that the thyroid of mice appears as two lobes without an isthmus. Bilateral recurrent nerve damage is fatal. However, the recurrent laryngeal nerve was located posterior to the thyroid lobe along with thyroid feeding vessels inside the pretracheal fascia (Fig. 3a), and they ascended toward the lateral aspect of the trachea just anterior to the angle between the trachea and esophagus up to the level of the cricoid cartilage (Fig. 3b). Thus, careful examination and use of a sophisticated technique can avoid fatal nerve damage. The neck anatomy of a mouse is comprised of compartments similar to that of humans (Fig. 4c). Thyroid glands are located in a visceral compartment posterior to the anterior neck muscles, and most major blood vessels are located in a carotid space. Therefore, careful dissection of the thyroid is feasible without massive bleeding. Minor bleeding from the thyroid artery or vein can be easily controlled by gentle pressure with a piece of cotton [9].

Postoperative care is critical to ensure full recovery after surgery. A warming lamp, oxygen supplementation, and fluid infusion are important preventive tools for postoperative morbidity and mortality [10]. Food was placed in the cage bottom for easy access. Compared with other surgical techniques, total thyroidectomy can cause hypoparathyroidism because of the resection of the adjacent parathyroid glands, so continuous calcium supplementation is important.

The relatively high mortality can be a problem and might be caused by surgical stress. There was no definite evidence of hemorrhage or recurrent laryngeal nerve injury in the fatal cases, which was confirmed by the postmortem examination. Excessive surgical stress results in a disruption of the homeostasis of the body and is known to cause various postoperative complications. Usually the surgical method, operation time, and intraoperative blood loss, etc., have been regarded as related surgical stresses and closely associated with the postoperative morbidity and mortality [11, 12]. Other studies have reported that changes in the neuroendocrine or immune responses reflect the degree of surgical stress [13–20]. It is not easy to predict the amount of surgical stress in each organism, because the physiological responses are variable, even when the factors associated with surgical stress remain the same [12]. Considering the fact that the mice included in our study were young and limited in number, the surgical stress could have been a cause of the mortality. By minimizing the factors related to surgical stress, an improved survival rate could be acquired.

Conclusion

Using our total thyroidectomy protocol, we successfully established a hNIS-transfected prostate cancer model with a minimal accumulation of radioiodine in the neck. The relatively high mortality after surgery can be a problem, and this might be reduced by minimizing the surgical stress.

Acknowlegements This work was financially supported by NCC Korea Intramural Grants 0710072-2 and 0910031-2.

Conflict of Interest Statement We declare that we have no conflict of interest.

References

1. Spitzweg C, Baker CH, Bergert ER, O'Connor MK, Morris JC. Image-guided radioiodide therapy of medullary thyroid cancer after carcinoembryonic antigen promoter-targeted sodium iodide symporter gene expression. Hum Gene Ther. 2007;18:916–24.
2. Spitzweg C, Zhang S, Bergert ER, Castro MR, McIver B, Heufelder AE, et al. Prostate-specific antigen (PSA) promoter-driven androgen-inducible expression of sodium iodide symporter in prosate cancer cell lines. Cancer Res. 1999;59:2136–41.
3. Kakinuma H, Bergert ER, Spitzweg C, Cheville JC, Lieber MM, Morris JC. Probasin promoter (ARR(2)PB)-driven, prostate specific expression of the human sodium iodide symporter (h-NIS) for targeted radioiodine therapy of prostate cancer. Cancer Res. 2003;63:7840–4.
4. Chung JK. Molecular nuclear medicine using sodium/iodide symporter. Int Congr Ser. 2004;1264:77–83.
5. Sultan M, Schulz MH, Richard H, Magen A, Klingenhoff A, Scherf M, et al. A global view of gene activity and alternative splicing by deep sequencing of the human transcriptome. Science. 2008;321:956–60.
6. Spitzweg C, Harrington KJ, Pinke LA, Vile RG, Morris JC. Clinical review 132: The sodium/iodide symporter and its potential role in cancer therapy. J Clin Endocrinol Metab. 2001;86:3327–35.

7. Sakurai MK, Greene AK, Wilson J, Fauza D, Puder M. Pneumonectomy in the mouse: Technique and perioperative management. J Invest Surg. 2005;18:201–5.
8. Gleave M, Hsieh JT, Gao CA, von Eschenbach AC, Chung LW. Acceleration of human prostate cancer growth in vivo by factors produced by prostate and bone fibroblasts. Cancer Res. 1991;51:3753–61.
9. Tarnavski O, McMullen JR, Schinke M, Nie Q, Kong S, Izumo S. Mouse cardiac surgery: comprehensive techniques for the generation of mouse models of human diseases and their application for genomic studies. Physiol Genomics. 2004;16:349–60.
10. Palacios-Romero R, Mowbray J. Evidence for the rapid direct control both in vivo and in vitro of the efficiency of oxidative phosphorylation by 3, 5, 3'-tri-iodo-L-thyronine in rats. Biochem J. 1979;184:527–38.
11. Ishibashi S, Takeuchi H, Fujii K, Shiraishi N, Adachi Y, Kitano S. Length of laparotomy incision and surgical stress assessed by serum IL-6 level. Injury. 2006;37:247–51.
12. Takenaka K, Ogawa E, Wada H, Hirata T. Systemic inflammatory response syndrome and surgical stress in thoracic surgery. J Crit Care. 2006;21:48–53.
13. Leung KL, Lai PB, Ho RL, Meng WC, Yiu RY, Lee JF, et al. Systemic cytokine response after laparoscopic-assisted resection of rectosigmoid carcinoma: a prospective randomized trial. Ann Surg. 2000;231:506–11.
14. Nishiguchi K, Okuda J, Toyoda M, Tanaka K, Tanigawa N. Comparative evaluation of surgical stress of laparoscopic and open surgeries for colorectal carcinoma. Dis Colon Rectum. 2001;44:223–30.
15. Members of the American College of Chest Physicians/Society of Critical Care Medicine Consensus Conference Committee. American College of Chest Physicians/Society of Critical Care Medicine Consensus Conference: Definitions for sepsis and organ failure and guidelines for the use of innovative therapies in sepsis. Crit Care Med. 1992;20:864–74.
16. Pittet D, Rangel-Frausto S, Li N, Tarara D, Costigan M, Rempe L, et al. Systemic inflammatory response syndrome, sepsis, severe sepsis and septic shock: incidence, morbidities and outcomes in surgical ICU patients. Intensive Care Med. 1995;21:302–9.
17. Smail N, Messiah A, Edouard A, Descorps-Declère A, Duranteau J, Vigué B, et al. Role of systemic inflammatory response syndrome and infection in the occurrence of early multiple organ dysfunction syndrome following severe trauma. Intensive Care Med. 1995;21:813–6.
18. Yim AP, Wan S, Lee TW, Arifi AA. VATS lobectomy reduces cytokine responses compared with conventional surgery. Ann Thorac Surg. 2000;70:243–7.
19. Nagahiro I, Andou A, Aoe M, Sano Y, Date H, Shimizu N. Pulmonary function, postoperative pain, and serum cytokine level after lobectomy: a comparison of VATS and conventional procedure. Ann Thorac Surg. 2001;72:362–5.
20. Grande M, Tucci GF, Adorisio O, Barini A, Rulli F, Neri A, et al. Systemic acute-phase response after laparoscopic and open cholecystectomy. Surg Endosc. 2002;16:313–6.